

# $H_0$ from an orientation-unbiased sample of SZ and X-ray clusters

Michael E. Jones,<sup>1</sup> Alastair C. Edge,<sup>2</sup> Keith Grainge,<sup>1</sup> William F. Grainger,<sup>1</sup>  
 Rüdiger Kneissl,<sup>1</sup> G.G. Pooley,<sup>1</sup> Richard Saunders,<sup>1</sup> Shigeru J. Miyoshi,<sup>3</sup>  
 Taisuke Tsuruta,<sup>3</sup> Koujun Yamashita,<sup>4</sup> Yuzuru Tawara,<sup>4</sup> Akihiro Furuzawa,<sup>4</sup>  
 Akihiro Harada,<sup>4</sup> Isamu Hatsukade<sup>5</sup>

<sup>1</sup>*Astrophysics Group, Cavendish Laboratory, Madingley Road, Cambridge CB3 0HE*

<sup>2</sup>*Department of Physics, South Road, Durham DH1 3LE*

<sup>3</sup>*Department of Physics, Kyoto Sangyo University, Kamigamo-Motoyama, Kita-ku, Kyoto 603-8555, Japan*

<sup>4</sup>*Department of Astrophysics, Faculty of Science, Nagoya University, Chikusa-ku, Nagoya 464-0814, Japan*

<sup>5</sup>*Faculty of Engineering, Miyazaki University, 1-1 Gakuen-kibanadai-nishi, Miyazaki 889-2192, Japan*

31 October 2018

## ABSTRACT

We have observed the Sunyaev–Zel’dovich effect in a sample of five moderate-redshift clusters with the Ryle Telescope, and used them in conjunction with X-ray imaging and spectral data from *ROSAT* and *ASCA* to measure the Hubble constant. This sample was chosen with a strict X-ray flux limit using both the BCS and NORAS cluster catalogues to be well above the surface-brightness limit of the *ROSAT* All-Sky Survey, and hence to be unbiased with respect to the orientation of the cluster. This controls the major potential systematic effect in the SZ/X-ray method of measuring  $H_0$ . Taking the weighted geometric mean of the results and including the main sources of random error, namely the noise in the SZ measurement, the uncertainty in the X-ray temperatures and the unknown ellipticity of the clusters, we find  $H_0 = 59^{+8}_{-7} \text{ km s}^{-1} \text{ Mpc}^{-1}$  assuming a standard CDM model with  $\Omega_M = 1.0, \Omega_\Lambda = 0.0$ , or  $H_0 = 65^{+8}_{-7} \text{ km s}^{-1} \text{ Mpc}^{-1}$  if  $\Omega_M = 0.3, \Omega_\Lambda = 0.7$ .

## Key words:

cosmic microwave background – cosmology:observations – X-rays – distance scale – galaxies:clusters:individual (A697, A773, A1413, A1914, A2218)

## 1 INTRODUCTION

It has long been recognised that the Sunyaev–Zel’dovich (SZ) effect (Sunyaev & Zel’dovich 1972) in clusters of galaxies, along with X-ray measurements, can provide a method of measuring distances on cosmological scales (Gunn 1978; Silk & White 1978; Cavaliere et al. 1979; Birkinshaw 1979). The method takes advantage of the differing dependences on the cluster electron density  $n_e$  and temperature  $T_e$  of the X-ray bremsstrahlung ( $\propto n_e^2 T_e^{1/2}$ ) and SZ effect ( $\propto n_e T_e$ ) to measure the physical size of the cluster, and hence its angular-diameter distance. The dependence of the derived value of  $H_0$  on the important quantities is

$$H_0 \propto \left( \frac{T_e}{\Delta T_{\text{SZ}}} \right)^2 \theta S_X \frac{\ell_\perp}{\ell_\parallel},$$

where  $\Delta T_{\text{SZ}}$  is the SZ brightness decrement,  $S_X$  is the X-ray surface brightness,  $\theta$  is the apparent angular size of the cluster, and  $\frac{\ell_\perp}{\ell_\parallel}$  is the ratio of the linear sizes of the cluster perpendicular and parallel to the line of sight.

The systematic effects in this method of measuring  $H_0$  are

quite different from those in other methods, either in the traditional distance ladder or in other direct physical methods such as gravitational lensing, and are mostly due to the difficulty of modelling the cluster gas that causes both the SZ effect and the X-ray emission. Recent work has shown that the small-scale features in the gas distribution such as cooling flows or clumping contribute smaller biases than might have been thought, since the effects on the observed quantities entering  $H_0$  tend to cancel each other even for a single cluster (eg, Grainger (2001), Maggi et al.). However, the large-scale distribution of the gas poses a problem, since the line-of-sight depth through the cluster cannot be measured directly, and has to be assumed to be the same as the size of the cluster in the plane of the sky. This assumption will be violated if clusters are chosen preferentially because of high surface brightness, since this will favour clusters that are extended along the line of sight. This will bias low the derived value of  $H_0$ . We therefore need a cluster sample that is selected on total flux rather than surface brightness, well above the surface brightness limit of the survey. Although several individual  $H_0$  estimates from the SZ/X-ray method have been published (eg (Hughes & Birkinshaw 1998; Holzapfel et al. 1997; Reese et al.

2000)), properly selected cluster samples are only recently beginning to emerge (Mason, Myers & Readhead 2001). In this paper we derive a sample of moderate-redshift X-ray-selected clusters that is carefully controlled to be free of any orientation bias, and use it to calculate  $H_0$  using the SZ data from the Ryle Telescope (RT).

Unless stated otherwise, we assume a standard cold dark matter cosmology (SCDM,  $\Omega_M = 1.0$ ,  $\Omega_\Lambda = 0.0$ ). We also give our results assuming a  $\Lambda$ CDM cosmology ( $\Omega_M = 0.3$ ,  $\Omega_\Lambda = 0.7$ ).

## 2 X-RAY CLUSTER SELECTION

The most complete X-ray cluster samples suitable for our purpose are selected from the *ROSAT* All-Sky Survey (RASS). We use two such samples, the Bright Cluster Sample (BCS) (Ebeling et al. 1998), and Northern Rosat All-Sky Survey (NORAS) (Böhringer et al. 2000). We began selection of our SZ sample from BCS while it was being compiled; we use NORAS as a consistency check. Both surveys are based on cluster candidates found in the first processing (SASS) of the RASS data, with further tests to check they are indeed clusters. A problem, particularly for clusters at high redshift, is the risk of incompleteness for compact clusters that may not appear extended enough to be recognised as such. BCS attempts to overcome this problem by adding known Abell and Zwicky clusters to the sample. However, comparing the BCS and NORAS samples after applying our RT selection criteria, it turns out that our sample is not affected by differences between the BCS and NORAS secondary selections.

The flux limit of NORAS is  $3 \times 10^{-12} \text{ erg s}^{-1} \text{ cm}^{-2}$  at 90% completeness; that of BCS is  $4.4 \times 10^{-12} \text{ erg s}^{-1} \text{ cm}^{-2}$  to the same completeness. But we limit our sample to even higher fluxes, of greater than  $5 \times 10^{-12} \text{ erg s}^{-1} \text{ cm}^{-2}$  (see Figure 1). Both this and a restriction to redshifts  $z < 0.3$  help reduce the risk of missing compact clusters. In accordance with the requirements for the Ryle Telescope we restrict our sample to the northern sky at declinations  $\delta > 20^\circ$ , to a redshift range of  $z > 0.14$ , and luminosities of  $L_x > 8 \times 10^{44} \text{ erg s}^{-1}$ . Table 1 lists the clusters from BCS and from NORAS that meet these criteria, and also indicates those which have radio sources that would make SZ measurement difficult or impossible. Where the surveys disagree on whether a cluster should be included on grounds of flux, we cautiously select only those clusters that meet our criteria in both surveys: this excludes three clusters above our flux limits in BCS and not in NORAS, and one in NORAS but not in BCS. This is consistent with the errors in the flux estimates in each survey. Two BCS-selected clusters are not in NORAS, consistent with the inclusion of optically selected clusters in BCS that are not in NORAS due to lack of extent. Of the eleven clusters satisfying our X-ray criteria, six have radio sources in the cluster or within the field of view of the RT that are too bright at 15 GHz to allow SZ observation with the RT. We have observed the remaining five, A697, A773, A1413, A1914 and A2218 with the RT and obtained detections for all of them; the results are discussed below. Since the presence of radio sources cannot be correlated with cluster orientation, this subsample is effectively randomly chosen, and therefore retains the orientation-independence of the whole sample. Indeed, we have checked that the our subsample is not correlated to X-ray properties such as flux, extent likelihood and measured extent. It therefore appears unlikely that any significant bias, larger than the random error, is present in our averaged  $H_0$  result. Clearly a larger sample would improve matters: the small size of our sample highlights the difficulty of selecting rig-

orously at moderately high redshift, even using the best large-area X-ray surveys available.

## 3 SZ OBSERVATIONS AND $H_0$ CALCULATION

Details of our observational and modelling methods are given in Grainge et al. (2001a), Grainge et al. (2001b) and Grainger et al. (2001). We briefly summarise them here.

In each case we fit the *ROSAT* PSPC or HRI image using an ellipsoidal  $\beta$ -model, with  $\beta$ , the core radii in the plane of the sky,  $\theta_1$  and  $\theta_2$ , the position angle of the major axis, the position on the sky, and the central electron density  $n_0$  all as free parameters. The core radius in the line of sight is set to the geometric mean of the other two. A downhill simplex method is used to maximise the likelihood of the data given the model, using Poisson statistics. For the PSPC images we use the hard band (0.5–2 keV) in order to minimise the effect of Galactic absorption.

We remove contaminating radio sources by a maximum likelihood fit to the visibility data, simultaneously fitting the SZ decrement (using the X-ray-determined model, with a variable amplitude) and the sources. We include trial sources at all positions suggested either from the long baseline RT data or from other observations such as NVSS (Condon et al. 1998), and allow their positions and fluxes to vary in the fit. This allows us to remove the effects of sources whose existence is known from lower-frequency observations but whose brightness would not warrant a significant detection from the RT data alone.

Finally we take the source-subtracted data and compare them with mock SZ data derived from the X-ray model, taking into account the full response of the RT. We vary the normalisation of the mock data (equivalent to varying  $H_0$ ) and find the likelihood of the data, and then multiply by a prior that is uniform in log space (since  $H_0$  is a scale parameter) to find the peak and extent of the posterior probability distribution. We then apply corrections for the more exact relativistic form of the Compton  $y$  parameter (Challinor & Lasenby 1998), and small time-dependant variations from the nominal RT flux calibration scale (determined from VLA monitoring of our primary flux calibrators, 3C48 and 3C286), as well as adding in (in quadrature) estimates of the other main sources of error.

We now give details of the procedure for each of the five clusters. Two have been published more fully elsewhere (A773, Saunders et al. (2001) and A1413, Grainge et al. (2001b)) and are briefly summarised here; one (A2218) is a re-analysis of previously published data (Jones 1995); the other two (A697 and A1914) are new.

### 3.1 A697

A697 was observed with the *ROSAT* HRI on 1995 November 6 with a live time of 28.1 ks. We also observed it using ASCA during 1996 April in order to determine its temperature. Analysing both the GIS and SIS data using standard XSPEC tools, we find a temperature of  $8.0^{+0.6}_{-0.4} \text{ keV}$  (68% confidence), with a metallicity of  $0.24 \pm 0.07$  solar. Fitting to the *ROSAT* HRI data, we find the parameters given in Table 2. The HRI image, model and residuals are shown in Figure 2.

We observed A697 with the RT on 42 occasions between 1994 August 6 and 1996 April 27. The map of all the data is shown in Figure 4. The bright source to the NW is extended, but can be successfully modelled as three point sources. Fitting simultaneously to the sources and SZ decrement gives a good fit

with the source parameters listed in Table 3. Fitting the source-subtracted data to the model derived from the X-ray data (Figure 3), and applying the relativistic and flux-scale corrections, we find  $H_0 = 52^{+8}_{-6} \text{ km s}^{-1} \text{ Mpc}^{-1}$  (errors from SZ fitting only). Including the other errors, dominated by the X-ray temperature ( $+14\%$ ) and ellipticity ( $\pm 14\%$ ), we find  $H_0 = 52^{+13}_{-11} \text{ km s}^{-1} \text{ Mpc}^{-1}$ . For a  $\Lambda$ CDM cosmology with  $\Omega_M = 0.3$  and  $\Omega_\Lambda = 0.7$ , this becomes  $H_0 = 59^{+15}_{-12} \text{ km s}^{-1} \text{ Mpc}^{-1}$ .

### 3.2 A773

Details of the determination of  $H_0$  from A773 are given in Saunders et al. (2001). We used a *ROSAT* HRI image and a temperature measurement from ASCA in conjunction with our RT data to estimate a value of  $H_0 = 77^{+19}_{-17} \text{ km s}^{-1} \text{ Mpc}^{-1}$  for SCDM,  $H_0 = 85^{+20}_{-19} \text{ km s}^{-1} \text{ Mpc}^{-1}$  for  $\Lambda$ CDM.

### 3.3 A1413

Details for A1413 are given by Grainge et al. (2001b), who also discuss the contributions to the  $H_0$  error budget in general. Using a *ROSAT* PSPC image and ASCA temperature, we find  $H_0 = 57^{+23}_{-16} \text{ km s}^{-1} \text{ Mpc}^{-1}$  for SCDM,  $H_0 = 61^{+25}_{-17} \text{ km s}^{-1} \text{ Mpc}^{-1}$  for  $\Lambda$ CDM.

### 3.4 A1914

A1914 was observed with the *ROSAT* PSPC for 8.6 ks in 1992 July. There are several pieces of evidence to suggest that A1914 is undergoing a merger. The *ROSAT* image (see Figure 5) shows significant substructure in the core of the cluster, but no evidence of a cooling flow. The temperature, measured from an ASCA observation, is rather high at  $8.56 \pm 0.39 \text{ keV}$ . The POSS optical image shows two distinct groups of galaxies with no single dominant galaxy, and finally there is a diffuse steep-spectrum radio source to the NE of the cluster centre that is detected in the WENSS (300 MHz) (Rengelink et al. 1996) and NVSS (1.4 GHz) surveys. This raises the question of whether A1914 should be included in our sample, since it is possible that the cluster gas might be far from hydrostatic equilibrium and difficult to model. We choose to include it in our sample since simulations (Grainger 2001) show that even including clusters with large internal kinetic energies in their gas does not bias the sample average  $H_0$ . However, such clusters can have a large scatter about the mean value – this does appear to be the case with A1914 and also with A2218.

We fitted a  $\beta$  model to the *ROSAT* PSPC image with the parameters given in Table 2. The residuals (see Figure 2) were noticeably poorer than those from the fits to other clusters such as A1413; a Monte Carlo analysis shows that the hypothesis that the true structure is a  $\beta$  model and that the features seen result from Poisson noise can be rejected at the  $4\text{-}\sigma$  level. A1914 was observed with the RT on 19 occasions between 1996 March 6 and April 16; the full resolution radio image is shown in Figure 5. There are clearly several radio sources near the cluster centre, some of which are also detected in a VLA image (Figure 5). We used the VLA source positions and positions from a long-baseline RT image to estimate the fluxes of nine sources; the fluxes found and subtracted are shown in Table 3. Fitting the source-subtracted short-baseline data to the X-ray-based model (Figure 3) results in a value of  $H_0 = 119^{+42}_{-31} \text{ km s}^{-1} \text{ Mpc}^{-1}$  with errors just from the SZ fitting,

and  $H_0 = 119^{+46}_{-38} \text{ km s}^{-1} \text{ Mpc}^{-1}$  including the other sources of error. For  $\Lambda$ CDM this becomes  $H_0 = 129^{+51}_{-42} \text{ km s}^{-1} \text{ Mpc}^{-1}$ .

### 3.5 A2218

A2218 was the first cluster to be observed in the RT SZ programme (Jones et al. 1993), and has also been extensively observed in many wavebands, with SZ detections in the radio (eg Birkinshaw & Hughes (1994)) as well as strong and weak lensing observations (eg Kneib et al. (1995) and Squires et al. (1996)) and X-ray studies (eg Markevitch (1997)). We have previously reported a measurement of  $H_0$  from this cluster (Jones 1995); we re-analyse our data here because we have improved our source-subtraction and modelling techniques, and because a new temperature measurement from ASCA is available that supersedes the previous GINGA measurement.

Figure 6 shows the image made by combining 30 days' RT data taken in two array configurations between 1992 December 4 and 1993 March 23. This map has simply been CLEANed with no source subtraction; nevertheless, even at this high resolution the SZ decrement is clearly visible, and an approximate calculation of the observed temperature decrement, using the CLEAN restoring beam size of  $40'' \times 36''$ , gives a maximum decrement of  $-760 \pm 150 \mu\text{K}$ . This agrees well with the fitted  $\beta$ -model central temperature of  $-797 \mu\text{K}$ .

We used the *ROSAT* PSPC observation made on 1991 May 25, which has a live time of 42.47 ks. The X-ray model fitting parameters are shown in Table 2. As with A1914, the X-ray image contains substructure that is significantly different from a smooth ellipsoidal  $\beta$  model (see Figure 2). Preliminary source subtraction in the map plane had shown that, of the three bright sources evident in Figure 6, the central one was point-like but the eastern and western sources had some additional extended flux. We therefore fitted a total of six trial sources, modelling the western source as three points and the eastern source as two. This gave a good fit to the data with the source parameters listed in Table 3. Subtracting these sources and fitting to the X-ray model (using an ASCA-derived temperature of  $7.20 \pm 0.36 \text{ keV}$  (Mushotzky & Loewenstein 1997)), we find a best fit value of  $H_0 = 31^{+8}_{-6} \text{ km s}^{-1} \text{ Mpc}^{-1}$ , where these errors only include the SZ fitting. Including the other dominant sources of error ( $\pm 10\%$  from the temperature measurement and  $\pm 14\%$  from the likely ellipticity), we find  $H_0 = 31^{+10}_{-8} \text{ km s}^{-1} \text{ Mpc}^{-1}$ , or  $H_0 = 35^{+11}_{-9} \text{ km s}^{-1} \text{ Mpc}^{-1}$  for  $\Lambda$ CDM.

### 3.6 Combined result

The values of  $H_0$  derived from each cluster are summarised in Table 4. Since the main sources of error in each value are in the form of a multiplicative factor, we calculate the sample mean by taking a weighted average of  $\log H_0$ . The result is  $H_0 = 59^{+8}_{-7} \text{ km s}^{-1} \text{ Mpc}^{-1}$  for SCDM or  $H_0 = 65^{+8}_{-7} \text{ km s}^{-1} \text{ Mpc}^{-1}$  for  $\Lambda$ CDM. Looking at the scatter in our individual values, we see that A697, A773 and A1413 all agree with the mean within  $1\text{-}\sigma$ . A1914 is  $1.6 \sigma$  above the mean and A2218 is  $2.8 \sigma$  below it. These are the two clusters for which there is independent evidence, from the lack of a good fit of the X-ray model and from the optical galaxy distribution, of significant dynamical activity. Since our error estimate does not include a component to take account of this effect (for lack of a means of quantifying it), it is not surprising that the scatter appears anomalously large. Nevertheless we feel justified in keeping these two clusters in the sample based on the evidence from simulations that

dynamically active clusters do not bias the value of  $H_0$  – indeed, removing them does not significantly change the best estimate of  $H_0$ .

#### 4 CONCLUSIONS

We have used *ROSAT* and *ASCA* X-ray data and Ryle Telescope SZ observations to measure the Hubble constant  $H_0$  from a sample of five clusters, selected using the BCS and NORAS cluster catalogues to be free of orientation bias. The weighted geometric mean value of  $H_0$  from this sample is  $H_0 = 59_{-7}^{+8} \text{ km s}^{-1} \text{ Mpc}^{-1}$  assuming a standard CDM model with  $\Omega_M = 1.0, \Omega_\Lambda = 0.0$ , or  $H_0 = 65_{-7}^{+8} \text{ km s}^{-1} \text{ Mpc}^{-1}$  if  $\Omega_M = 0.3, \Omega_\Lambda = 0.7$ .

#### 5 ACKNOWLEDGEMENTS

We thank the staff of the Cavendish Astrophysics group who ensure the operation of the Ryle Telescope, which is funded by PPARC. AE acknowledges support from the Royal Society; RK acknowledges support from an EU Marie Curie Fellowship; WFG acknowledges support from a PPARC studentship. We have made use of the *ROSAT* Data Archive of the Max-Planck-Institut für extraterrestrische Physik (MPE) at Garching, Germany. We thank Hans Böhringer for helpful discussions.

**REFERENCES**

- Birkinshaw M., 1979, MNRAS, 187, 487
- Birkinshaw M., Hughes J. P., ApJ, 1994, 420, 33.
- Bohringer H., Voges W., Huchra J.P., McLean B., Giacconi R., Rosati P., Burg R., Mader J., Schuecker P., Simic D., Komossa S., Reiprich T.H., Retzlaff J., Trumper J., 2000, ApJS, 129, 435.
- Cavaliere A., Danese L., DeZotti G., 1979, A&A, 75, 322.
- Challinor A., Lasenby A. N., ApJ, 1998, 499, 1.
- Condon J.J., Cotton W.D., Greisen E.W., Yin Q.F., Perley R.A., Taylor G.B., Broderick J.J., 1998, AJ, 115, 1693.
- Ebeling H., Edge A.C., Bohringer H., Allen S.W., Crawford C.S., Fabian A.C., Voges W., Huchra J.P., 1998, MNRAS, 301, 881.
- Grainge K., Grainger W. F., Jones M. E., Kneissl R., Pooley G. G., Saunders R., 2001a, submitted to MNRAS.
- Grainge K., Jones M. E., Saunders R., Pooley G. G., Edge A., Kneissl R., 2001b, submitted to MNRAS.
- Grainger W. F., 2001, PhD. thesis, University of Cambridge.
- Grainger W. F., Das R., Grainge K., Jones M. E., Kneissl R., Pooley G. G., Saunders R., 2001, submitted to MNRAS.
- Gunn J.E., 1978, in: Observational Cosmology, ed. A. Maeder, L. Martinet and G. Tammann (Geneva: Geneva Observatory)
- Holzappel W. L., Arnaud M., Ade P. A. R., Church S. E., Fischer M. L., Mauskopf P. D., Rephaeli Y., Wilbanks T. M., Lange A. E., 1997 ApJ, 480, 449.
- Hughes J. P., Birkinshaw M., 1998, ApJ, 501, 1.
- Jones M. E., Saunders R., Alexander P., Birkinshaw M., Dillon N., Grainge K., Lasenby A., Lefebvre D., Pooley G. G., Scott P., Titterton D., Wilson D., 1993, Nat, 365, 320.
- Jones, M. E., 1995, Astro. Lett. and Communications, 1995, 32, 347.
- Kim K.T., Tribble P. C., Kronberg P. P., 1991, ApJ, 379, 80.
- Kneib J. P., Mellier Y., Pello R., Miralda-Escude J., Le Borgne J.-F., Bohringer H., Picat J.-P., 1995, A&A, 303, 27.
- aggi A., et al., in prep
- Markevitch M., 1997, ApJL, 483, L17.
- Markevitch, M., Forman, W. R., Sarazin, C.L., Vikhlinin, A., ApJ, 1998, 503, 77
- Mason, B.S., Myers, S. T., Readhead, A. C. S., 2001, ApJL in press (astro-ph/0101169). 485, 1.
- Mushotzky R.F., Loewenstein M., 1997, ApJ, 481, L63.
- Myers, S. T., Baker, J. E., Readhead, A. C. S., Leitch, E. M., Herbig, T., 1997, ApJ, 485, 1.
- Reese E. D. , Mohr J. J., Carlstrom J. E., Joy M. , Grego L., Holder G. P., Holzappel W. L., Hughes J. P., Patel S. K., Donahue M., 2000, ApJ 533 38.
- Rengelink R.B, Tang Y., de Bruyn A.G., Miley G.K., Bremer M.N., Röttgering H.J.A., Bremer M.A.R., 1996, A&AS, 124, 259-28
- Saunders R., Kneissl R. , Grainger W. F., Grainge K., Jones M. E., Maggi A., Das R. Edge A. C., Lasenby A. N., Pooley G. G., Miyoshi S. J., Tsuruta T., Yamashita K., Tawara Y., Furuzawa A., Harada A., Hatsukade I., 2001, submitted to MNRAS.
- Silk J., White S.D.M., 1978, ApJL, 226, L103
- Squires G., Kaiser N., Babul A., Fahlman G., Woods D., Neumann D. M., Bohringer H., 1996, ApJ, 461, 572.
- Sunyaev R. A., Zel'dovich Ya B., 1972, Comm. Astrophys. Sp. Phys., 4, 173.

Cluster	Flux density ( $\mu\text{Jy}$ )	RA offset (arcsec)	dec offset (arcsec)
A697	462	-468	193
	154	-442	156
	215	-483	226
	624	28	-236
A1914	153	-262	-195
	379	-169	-99
	155	-141	31
	173	-108	201
	103	-118	-52
	278	-96	-82
	234	49	66
	123	-56	210
A2218	1438	-189	36
	1227	-40	117
	1541	126	94
	522	132	105
	543	-196	23
	240	-207	41

**Table 3.** Sources subtracted from the radio data. The flux densities given are apparent, ie not corrected for the RT primary beam. Offsets are from the radio pointing centres: A697  $08^{\text{h}}42^{\text{m}}57^{\text{s}}.7 + 36^{\circ}.721'45''$ ; A1914  $14^{\text{h}}26^{\text{m}}02^{\text{s}}.0 + 37^{\circ}49'29''$ ; A2218  $14^{\text{h}}26^{\text{m}}02^{\text{s}}.0 + 37^{\circ}49'29''$  (J2000). The errors on the source fluxes are  $\pm 30$ ,  $\pm 45$  and  $\pm 35 \mu\text{Jy}$  respectively.

Cluster	$H_0$ (SCDM)	$H_0$ ( $\Lambda$ CDM)	$\Delta T_0$ ( $\mu\text{K}$ )
A697	$52^{+13}_{-11}$	$59^{+15}_{-12}$	1047
A773	$77^{+19}_{-17}$	$85^{+20}_{-19}$	737
A1413	$57^{+23}_{-16}$	$61^{+25}_{-17}$	863
A1914	$119^{+46}_{-38}$	$129^{+51}_{-42}$	864
A2218	$31^{+10}_{-8}$	$35^{+11}_{-9}$	797
Sample	$59^{+8}_{-7}$	$65^{+8}_{-7}$	

**Table 4.**  $H_0$  values for the five clusters in the sample, for both SCDM and  $\Lambda$ CDM cosmologies. Also given are the central temperature decrements using the best normalisation of the fitted  $\beta$  model to the SZ data.

Cluster	R.A. (J2000)	Dec	$z$	$f_X^{\text{BCS}}$	$L_X^{\text{BCS}}$	$f_X^{\text{NORAS}}$	$L_X^{\text{NORAS}}$	B?	N?	R?
A586	113.091	31.629	0.1710	9.1	11.12	7.94	9.84	*	*	
A665	127.739	65.854	0.1818	11.8	16.33	11.23	15.69	*	*	
<b>A697</b>	130.741	36.365	0.2820	5.0	16.30	5.77	19.15	*	*	*
<b>A773</b>	139.475	51.716	0.2170	6.7	13.08	5.71	12.11	*	*	*
Z2701	148.198	51.891	0.2140	5.6	10.68	–	–	*		
A963	154.255	39.029	0.2060	5.9	10.41	–	–	*		
<b>A1413</b>	178.826	23.408	0.1427	15.5	13.28	12.69	10.91	*	*	*
A1423	179.342	33.632	0.2130	5.3	10.03	3.73	7.23	*		*
A1682	196.739	46.545	0.2260	5.3	11.26	4.07	8.79	*		
A1758	203.179	50.550	0.2799	3.6	11.68	5.60	18.29		*	*
A1763	203.818	40.996	0.2279	6.9	14.93	6.35	13.85	*	*	
<b>A1914</b>	216.509	37.835	0.1712	15.0	18.39	12.90	15.91	*	*	*
A2111	234.924	34.417	0.2290	5.0	10.94	3.91	8.68	*		
<b>A2218</b>	248.970	66.214	0.1710	7.5	9.30	7.16	8.16	*	*	*
A2219	250.094	46.706	0.2281	9.5	20.40	11.18	24.33	*	*	
RXJ1720	260.037	26.635	0.1640	14.3	16.12	10.84	12.34	*	*	
A2261	260.615	32.127	0.2240	8.7	18.18	9.83	20.61	*	*	

**Table 1.** The selection of the cluster sample from the BCS and NORAS surveys. Clusters are required to have  $L_X > 8 \times 10^{44} \text{ergs}^{-1}$  and  $f_X > 5 \times 10^{-12} \text{ergs}^{-1} \text{cm}^{-2}$  in both samples, and to be free of contaminating radio sources. The final three columns indicate which clusters are selected from BCS, NORAS, and radio data respectively. Eleven clusters meet the X-ray selection criteria, and five of these (shown in bold) are sufficiently free of radio sources to have their SZ effects measured. Units of luminosity  $L_X$  are  $10^{44} \text{ergs}^{-1}$  and of flux  $f_X$  are  $10^{-12} \text{ergs}^{-1} \text{cm}^{-2}$ .

Cluster	$z$	$\beta$	$\theta_1$ (")	$\theta_2$ (")	PA $^\circ$	$n_0 h_{50}^{-1/2} \text{cm}^{-3}$	Temperature (keV)
A697	0.282	0.67	46	34	101	$7.9 \times 10^{-3}$	$8.0^{+0.55}_{-0.42}$
A773	0.217	0.64	61	44	16	$6.8 \times 10^{-3}$	$8.7^{+0.42}_{-0.42}$
A1413	0.143	0.58	56	38	1	$9.6 \times 10^{-3}$	$8.5^{+0.79}_{-0.48}$
A1914	0.1712	0.69	51	46	10	$13.6 \times 10^{-3}$	$8.6^{+0.36}_{-0.39}$
A2218	0.171	0.65	69	53	-8	$6.0 \times 10^{-3}$	$7.20^{+0.36}_{-0.36}$

**Table 2.** X-ray parameters for the five clusters used in the combined  $H_0$  measurement.

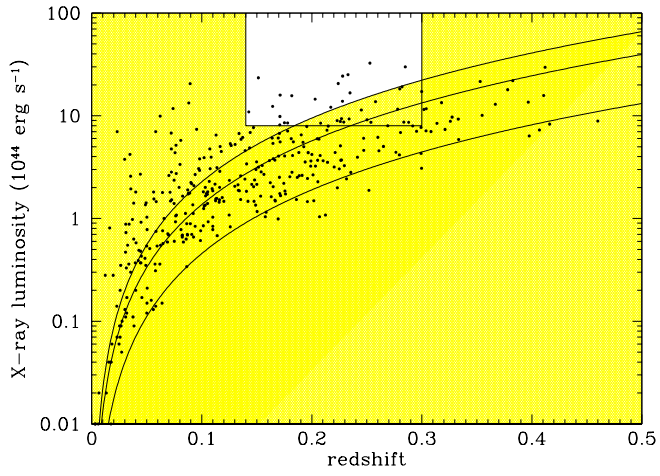


**Figure 1.** The full NORAS X-ray cluster sample and the region (white) of our SZ subsample. The lines correspond to flux limits of  $1$ ,  $3$  and  $5 \times 10^{-12}$   $\text{erg s}^{-1} \text{cm}^{-2}$ , which are the approximate lower detection limit, the 90% completeness limit, and the limit of the SZ sample respectively.



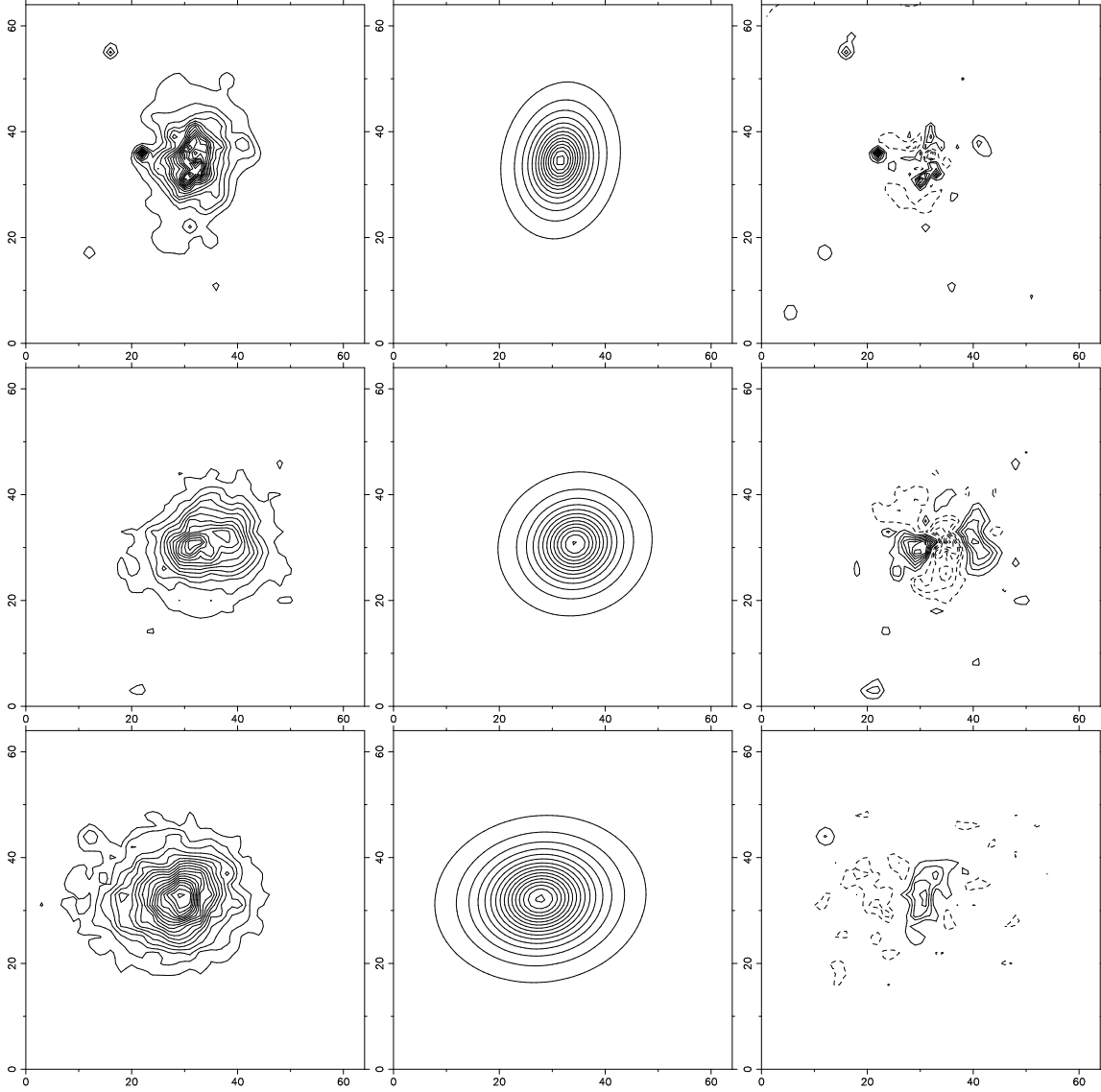


**Figure 2.** X-ray image, best-fitting model, and residuals for (top) A697, (centre) A1914 and (bottom) A2218. The contour intervals are respectively 1 count per 4 arcsec pixel, 2 counts per 8 arcsec pixel and 2 counts per 8 arcsec pixel.

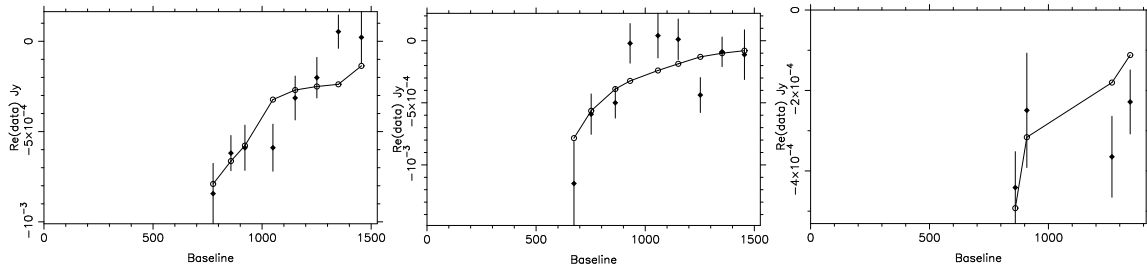


**Figure 3.** Source-subtracted visibilities (real part only) for (left) A697, (centre) A1914 and (right) A2218 (filled points with error bars), binned azimuthally, compared with the best-fitting model in each case (open points joined by lines). The lack of smoothness in the models is due to the inclusion of points from different baselines with different model values (due to ellipticity) in the same bin.

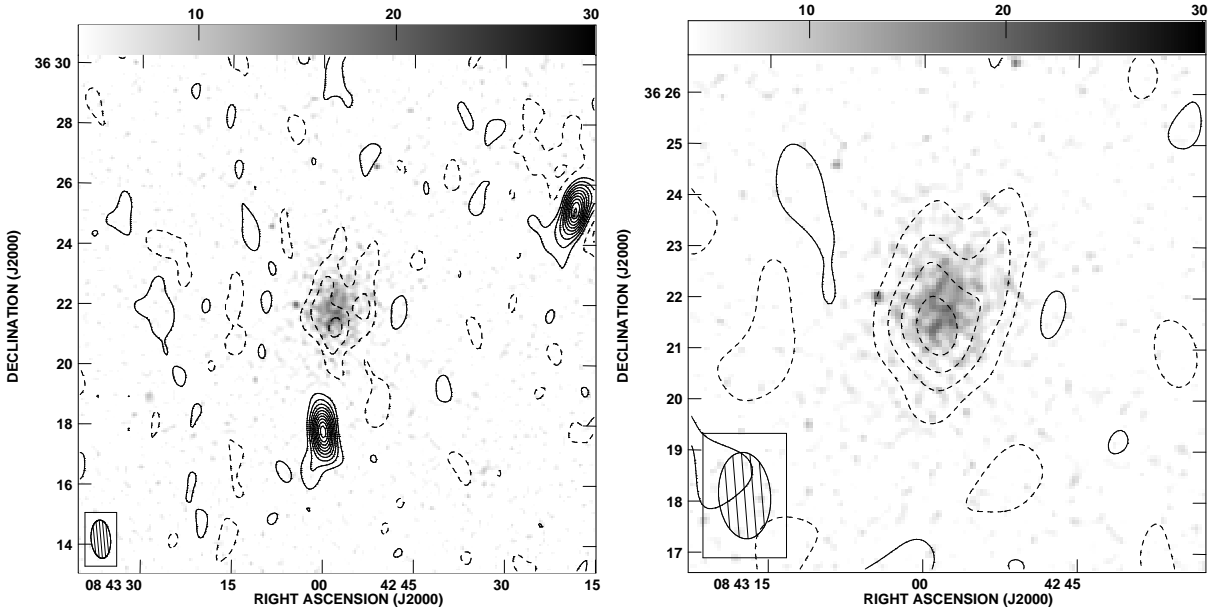


**Figure 4.** (Left) CLEANed map of all the radio data on A697 (contours) superposed on the *ROSAT* HRI image (greyscale). The contour interval is  $60 \mu\text{Jy beam}^{-1}$ ; dashed contours are negative. The CLEAN restoring beam of  $101'' \times 61''$  is shown (inset). (Right) CLEANed map of the source-subtracted radio data on A697, with a gaussian taper of width  $2000\lambda$  applied (contours) superposed on the *ROSAT* HRI image (greyscale). The contour interval is  $60 \mu\text{Jy beam}^{-1}$ ; dashed contours are negative. The CLEAN restoring beam of  $76'' \times 39''$  is shown (inset).

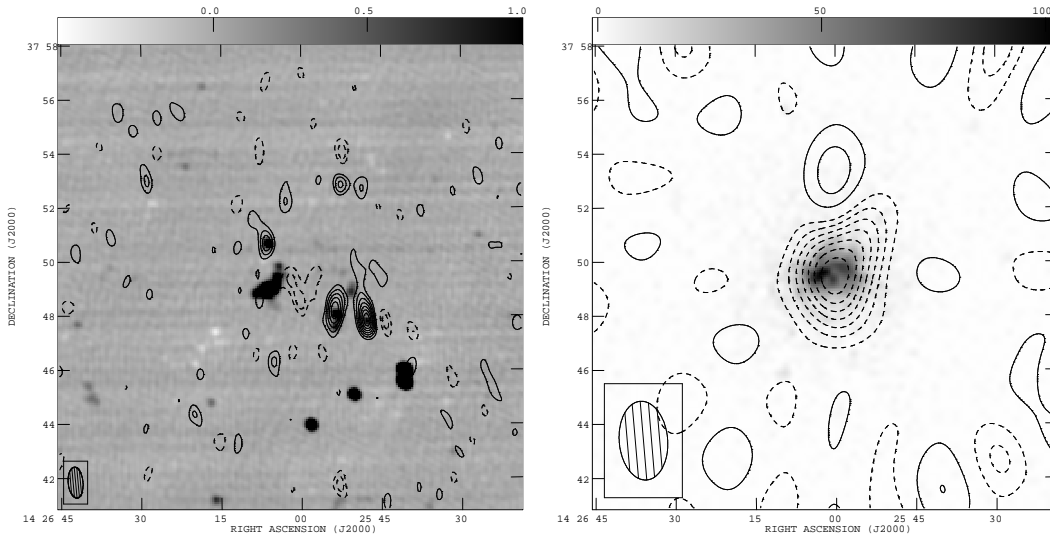


**Figure 5.** (left) Full-resolution radio image of A1914 (contours) overlaid on a VLA 1.4 GHz image (greyscale). The contours are at  $-3, -2, 2, 3, 4, 5, 6, 7, 8 \times 35 \mu\text{Jy beam}^{-1}$ ; the beamsize of  $69 \times 33$  arcsec, PA  $5^\circ$  is shown (inset). The steep-spectrum halo source can be seen in the VLA image just to the east of the cluster centre – no emission is apparent in the RT image however, where the SZ decrement can also be seen. (right) Source-subtracted CLEANed low-resolution radio image of A1914 showing the SZ decrement, overlaid on the *ROSAT* PSPC image (greyscale). The contour interval is  $80 \mu\text{Jy beam}^{-1}$ , dashed contours are negative. The beam (inset) is  $175'' \times 108''$ , PA  $4^\circ$ .

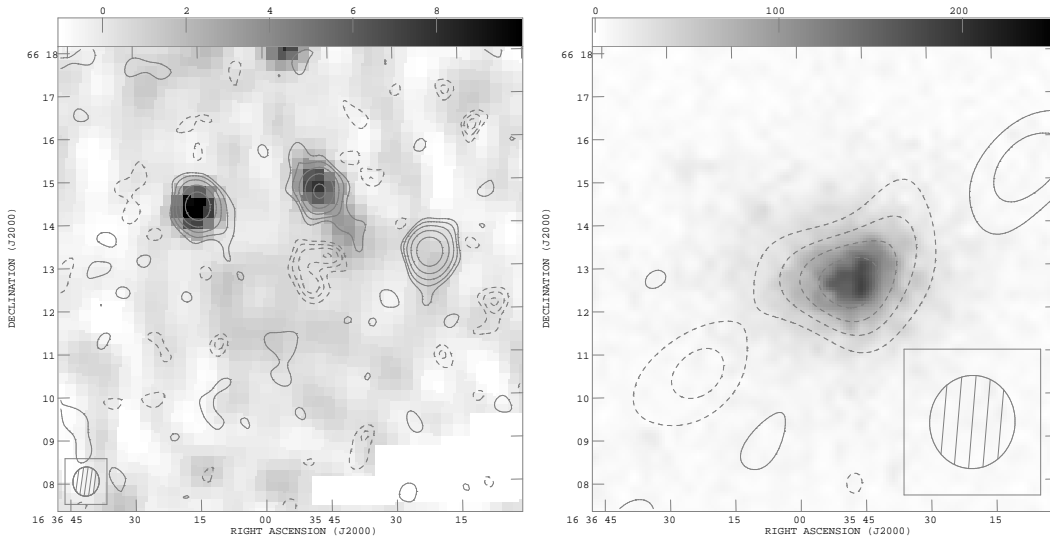


**Figure 6.** (left) Full-resolution radio image of A2218 (contours) overlaid on the NVSS 1.4 GHz image (greyscale). The contours are at  $-4, -3, -2, 2, 4, 8, 16, 32 \times 35 \mu\text{Jy beam}^{-1}$ ; the beamsize of  $41 \times 36$  arcsec, PA  $-9^\circ$  is shown (inset). The SZ decrement can be clearly seen even in this high-resolution image. (right) Source-subtracted CLEANed low-resolution radio image of A2218 showing the SZ decrement, overlaid on the ROSAT PSPC image (greyscale). The contours interval is  $80 \mu\text{Jy beam}^{-1}$ , dashed contours are negative. The beam (inset) is  $130'' \times 120''$ , PA  $-5^\circ$ .